

Novel manufacturing method for highly flexible poly(lactic acid) foams and ferroelectrets

Dániel Vadas^a, Katalin Bocz^{a,*}, Tamás Igricz^a, János Volk^b, Sándor Bordács^{c,d},
Lajos Madarász^a, György Marosi^a

^a Department of Organic Chemistry and Technology, Faculty of Chemical Technology and Biotechnology, Budapest University of Technology and Economics, Műgyetem rkp. 3, H-1111, Budapest, Hungary

^b Centre for Energy Research, Institute of Technical Physics and Materials Science, Konkoly-Thege M. u. 29-33, H-1121, Budapest, Hungary

^c Department of Physics, Institute of Physics, Budapest University of Technology and Economics, Műgyetem rkp. 3, H-1111, Budapest, Hungary

^d ELKH-BME Condensed Matter Research Group, Budapest University of Technology and Economics, Műgyetem rkp. 3., H-1111 Budapest, Hungary

ARTICLE INFO

Article history:

Received 3 February 2023

Received in revised form

21 March 2023

Accepted 26 March 2023

Keywords:

Flexible PLA foam

Anisotropy

Structural elasticity

Ferroelectret

ABSTRACT

Poly (lactic acid) (PLA) foams have demonstrated a high variety of functional characteristics, still, the rigidity of this cellular material remains a major limiting factor when it comes to implementation options. In this contribution, PLA foams with outstanding flexibility were created for the first time by a new approach of uniaxial stretching and immediate relaxation following supercritical CO₂-assisted extrusion foaming. Instead of improving the resilience of the PLA raw material, structural elasticity of the foam was achieved via altering the deformation mechanism from cell wall collapse or rupture towards reversible and extensive flexural strain. In addition, PLA foams with excellent piezoelectric properties were also achieved via high-voltage corona poling, giving additional function to the lens-like anisotropic foam cells. This foaming technology creates the opportunity to produce PLA piezoelectrets in a way entirely different from the state-of-the-art methods. Correlation between the tensile as well as compression elongations and moduli, cell morphology and longitudinal piezoelectric coefficients (d_{33}) of electretized foam samples were studied. Unprecedented reversible tensile elongations of up to 16% and total elongations of up to 35% were reached, as well as considerable d_{33} values in the range of 50–320 pC/N were obtained for PLA ferroelectrets.

© 2023 Kingfa Scientific and Technological Co. Ltd. Publishing services by Elsevier B.V. on behalf of KeAi Communications Co. Ltd. This is an open access article under the CC BY license (<http://creativecommons.org/licenses/by/4.0/>).

1. Introduction

Efficiency has always been playing a vital role in our continuously developing civilization, additionally, growing environmental awareness has drawn more attention to advanced sustainable solutions [1]. From time to time, an unexpected energy crisis also puts the topic in the spotlight, underlining the economic benefits of eco-friendly products more clearly. For a newly developed product to be considered eco-friendly or “green”, it is not sufficient to only sound good or to be marketable, but its performance has to be evaluated rigorously by life cycle assessment (LCA) methods [2]. With regard to the inevitable scarcity of fossil fuels, poly (lactic acid) (PLA), a biopolymer derived from renewable resources could be a major part of the solution in the long run according to LCA studies [3–10].

This polymer is the most extensively researched and utilized biodegradable aliphatic polyester due to its processability, recyclability, mechanical properties, and biocompatibility [11]. It is trigger-biodegradable, meaning that at ambient conditions it is chemically stable, however, when specific conditions are met ($T = 37\text{--}70\text{ }^{\circ}\text{C}$, $\text{PH} = 7\text{--}10$, presence of microorganisms, humidity, oxygen), PLA is designed to biodegrade within a few months [12].

Recognized as one of the most energy-efficient class of materials, polymeric foams have long been employed in a number of essential applications such as thermal and acoustic insulation [13–15], lightweight structural components [16–19], and energy absorption (packaging, cushioning, sports) [20–22]. Taking advantage of the environmentally beneficial properties of both biopolymers and gas-polymer composites (including foams), considerable scientific efforts have been made to develop processing technologies suitable for PLA as well [23,24]. When foamed, PLA usually forms a rigid closed-cell porous material, with physical characteristics and processing nature similar to expanded

* Corresponding author.

E-mail address: bocz.katalin@vbk.bme.hu (K. Bocz).

<https://doi.org/10.1016/j.aiepr.2023.03.005>

2542-5048/© 2023 Kingfa Scientific and Technological Co. Ltd. Publishing services by Elsevier B.V. on behalf of KeAi Communications Co. Ltd. This is an open access article under the CC BY license (<http://creativecommons.org/licenses/by/4.0/>).

polystyrene (EPS) [25]. The rigidity of PLA foams originates from the inherently low impact resistance of the polymer, having elongation at break lower than 15% [26]. As a consequence of the basic chemical structure, the elastic elongation range of foamed PLA is quite narrow. Cell walls undergo irreversible damage due to excessive static or dynamic stress [27], thus PLA foams with high reversible tensile or compressive deformation are very hard to manufacture.

Equipping cellular materials with different advanced functional properties is a popular research area, of which the effect of dimensional anisotropy is particularly noteworthy. By altering the aspect ratio of the foam cells, it is possible to improve the relevant (e.g. dielectric, thermal, mechanical) characteristics of the product [1,15,21,28–37]. Most of the studies emphasized the improved strength of the elongated foam cells in the orientation direction, focusing on increasing the elastic modulus of their anisotropic structure. All of the studies found in the literature produced such structures by uni- or biaxial orientation during the cell growth phase and subsequent stabilization of the foam cells. Consequently the cell wall membranes solidified while being elongated in the direction of the stretching force, provided by constrained autoclave foaming [15,31–33,36], die-opening foam injection molding [21,35] or extrusion foaming followed by uni- or biaxial orientation (i.e., blown-film process) [28,29,34,37]. An explanatory illustration of the state-of-the-art technologies is presented in Fig. 1a–c with regard to the feasible cell types with different aspect ratios. Although the cited anisotropic PLA cellular structures exhibited improved flexibility and decreased modulus during static tensile and compression tests, cyclic tests are rarely conducted with high dynamic range [27]. To the best of our knowledge, there is no evidence of highly flexible PLA foams in the scientific literature, more precisely those showing significant reversible tensile elongations. Accordingly, improving the resilience and flexibility of the otherwise fragile material would be of high importance. One promising way to achieve this is through exploiting size effect and structural (morphological) elasticity of thin and anisotropic cell walls, similarly to compliant mechanisms [38].

Along with the extensive set of beneficial properties originated in the special microstructure of polymer-based foams, advanced features are also being developed such as electromagnetic shielding [41], tissue engineering scaffolds [31], oil/water separation and self-cleaning characteristics [42], and so on. In particular, electro-mechanical effects have been the subject of increased research

interest [43–45], presupposing polymer foams to become the organic, lead-free, and thus less toxic substituents of polycrystalline $\text{Pb}(\text{Zr,Ti})\text{O}_3$ (PZT) based piezoelectric ceramics or single crystals [46]. These are functional materials that can convert mechanical deformation into electricity and vice versa [47]. Piezoelectret materials based on organic substances are manufactured by generation of charge carriers between a grounded and a corona electrode from the electric discharge of air, their injection into dielectric materials and their permanent capture by surface or volume traps [48]. A unique manufacturing technology of ferroelectric cellular materials was developed in Finland including biaxial orientation of an extrusion foamed tubular product which is then slit into flat foam sheets [43,49]. By means of high voltage corona poling, Paschen breakdown takes place in the voids [50]. During ionization, charge separation and their deposition occur on opposing sides of highly anisotropic individual cells, meanwhile the captured charges induce an additional electric field the direction of which is opposite to the electric field formed by the charging voltage, thus rendering the foam macroscopically piezoelectric [44,51]. Concerning the development of ferroelectrets during the last two decades, an uncomprehensive summary of the literature is presented in Table 1, pointing out the relevant parameters for electretization, cell morphology, and the measurement of piezoelectric coefficient (d_{33}). While this particular group of anisotropic foams showed improved flexibility and preferably decreased modulus during compression tests, there is no data on their tensile properties in the flexible (i.e., thickness) direction, as measurement of 10–200 μm thin samples would have been complicated and impractical.

PLA-based ferroelectrets are relatively new, only a few papers were published in this field [63,64]. Moreover, there is only a sole example of PLA foam applied as space charge electret [62]. Note that the inherent piezoelectric activity of crystalline PLA [47,60] is a completely different phenomenon and is not associated with the piezoelectricity of the space-charge electrets patented in 1987 using cellular PP film [43], and applied to PLA foams for the first time in 2020 [62]. Zhukov et al. used foamed PLA films most certainly obtained by biaxial orientation similarly to the PP ferroelectrets, followed by an additional hot pressing step.

In this work, a novel and cost-effective approach towards the manufacturing of anisotropic polymeric foams was implemented for the first time. Using supercritical CO_2 -assisted extrusion foaming line equipped with a belt puller, instead of stabilization of the PLA foam cells after orientation, the product was let to relax by

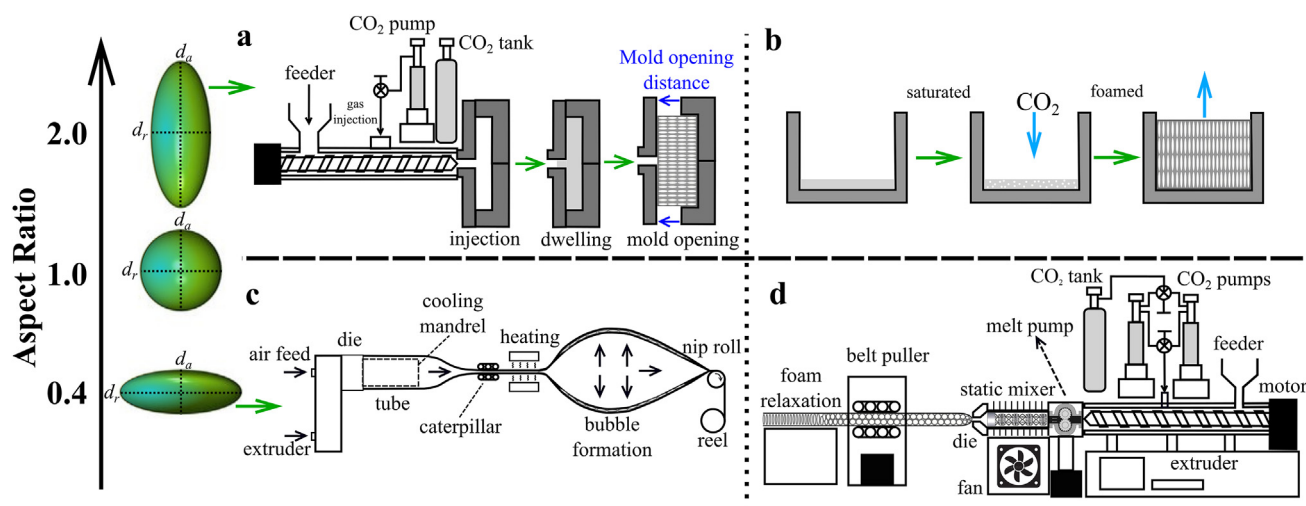


Fig. 1. Cell shapes for various aspect ratios and their manufacturing methods: a) die-opening injection molding [35]; b) constrained autoclave foaming; [36] c) extrusion & biaxial orientation (blown-film); [39] d) schematic drawing of the invented technology; [40].

Table 1

Summary of the scientific literature in the field of polymer-based electrets (U_p : poling voltage, E : elastic modulus, d_s : smaller diameter, d_l : larger diameter, d_{33} : piezoelectric coefficient).

Year	Polymer film	Manufacturing method	Electretization U_p [kV]; t [s]; D [mm]	E [MPa]	Aspect Ratio	Cell diameters (d_s ; d_l) [μ m]	d_{33} measuring method	d_{33} [pC/N]	Reference
1976	PVDF	uniaxial stretching	1.1 MV/cm; $t = 2$ h $T = 115$ °C	9470	N/A	N/A	complex electric admittance	17.4	Ohigashi et al. [52]
1987	PP	biaxial stretching	N/A	N/A	$3-5 \times 10^{-3}$	0.25; 50-80	N/A	N/A	Kirjavainen et al. [43,49]
2000	PTFE	biaxial stretching	$\pm 8-18$ kV; 30-90 min	N/A	0.1-?	1-5; 5-10	vibr. 1 kg	40-150	Künstler et al. [53]
2000	PP O01	biaxial stretching	20-30 kV; 2 s	N/A	0.01-0.5	1-5; 10-100	vibr.	30 ± 2	Paajanen et al. [44]
2000	PP HS01	biaxial stretching	20-30 kV; 2 s	N/A	0.02-0.9	2-9; 10-100	vibr.	170 ± 5	Paajanen et al. [44]
2001	PP O01	biaxial stretching	10-30 kV; 2-60s	9	0.01-0.5	1-5; 10-100	10 Hz; 100 kPa	28	Paajanen et al. [54]
2001	PP HS01	biaxial stretching	10-30 kV; 2-60s	0.89	0.02-0.9	2-9; 10-100	10 Hz; 100 kPa	170	Paajanen et al. [54]
2001	PP HT01	biaxial stretching	N/A	2.2	n.a.	-10; -100	period. 150 g	-250	Neugschwandtner et al. [55]
2004	PP VHD40	biaxial stretching	N/A	N/A	0.02-0.99	1-5 <10; <100	electro-acoustic	420	Hillenbrand et al. [51]
2004	PP VHD40/50	biaxial stretching	32 kV; 60 s	1.3-4.4	0.01-0.5	1-5; <100	1 Hz; 3.8 N	0-600	Zhang et al. [56]
2004	PP VHD40	biaxial stretching	-24 kV; 30 s	N/A	0.01-0.9	2-30; 5-60	vibr. 500 g	50-590	Wegener et al. [57]
2004	PP O01	biaxial stretching	N/A	0.8-10	0.01-0.9	1-5; 10-100	dielectric resonance	13-306	Wegener et al. [58]
2004	PP HS01	biaxial stretching	N/A	1-3	0.02-0.9	2-9; 10-100	dielectric resonance	46-108	Wegener et al. [58]
2005	PP EUH75	biaxial stretching	N/A	1.0	0.015-0.4	2-20; 10-130	few Hz	20-325	Qiu et al. [59]
2014	PLLA film	uni- or biaxial stretching	N/A	N/A	N/A	N/A	d_{14}	15-20	Ando et al. [60]
2021	PP	biaxial stretching	12-18 kV, 10 mm	N/A	0.006-0.6	3-30; 50-500	oscill.	160-280	Koike et al. [61]
2022	PLA	biaxial stretching, compression	-25 kV; 300 s; 50 mm	0.1-5	0.006-0.3	-30; 150-500	vibr: 10-1000 Hz; 20-225 g	200-250	Zhukov et al. [62]

the immediate elimination of the stretching force (Fig. 1d). The resulting highly flexible and anisotropic PLA foam was comprehensively characterized, including the investigation of its potential electromechanical applications. A patent application was filed regarding this innovative technology [40].

2. Experimental section

2.1. Materials

Ingeo™ Biopolymer 3052D type PLA ($M_w = 116,000$ g/mol, specific gravity: $\rho = 1.24$ g/cm³, $T_m = 145-160$ °C, melt flow index (MFI) of 14 g/10 min at 210 °C/2.16 kg), purchased from NatureWorks LLC (Minnetonka, MN, USA), was used. Joncryl ADR 4468 (BASF, Germany) was used as chain extender (CE) (a multifunctional epoxy-based styrene-acrylic oligomer, specific gravity: 1.08 g/cm³; glass transition temperature: 54 °C). Cloisite 116®, a non-treated montmorillonite (MMT) clay purchased from BYK-Chemie GmbH (Moosburg, Germany) was used as nucleating agent. A foaming compound comprising of 98.25 wt% PLA, 0.25 wt% CE, and 1.50 wt% MMT was prepared using a Labtech Scientific LTE 26-44 modular twin-screw extruder with a constant screw speed of 20 rpm (temperature profile of the extruder zones: zone₁ = 170 °C, zone₂₋₄ = 175 °C, zone₅₋₇ = 180 °C, zone₈₋₁₀ = 185 °C, die = 190 °C).

2.2. Methods

2.2.1. Extrusion foaming with uniaxial orientation and relaxation

LTE 26-44 (Labtech Engineering, Thailand) twin-screw extruder was used for the mixing with zone temperatures between 175 and 190 °C. Before each high-temperature processing step (i.e., compounding, foaming), the PLA pellets were dried for 8 h at 85 °C. Flexible PLA foams were produced by sc-CO₂ assisted extrusion foaming (Fig. 1d) on a modified Collin Teach-Line ZK 25 T type co-rotating twin-screw extruder (Dr Collin GmbH, Ebersberg, Germany) with a screw diameter of 25 mm and an L/D ratio of 30. The extruder has a total of 5 heating zones of which the initial 3 zones are responsible for plasticizing and melt transport, followed by the

4th zone in which sc-CO₂ is introduced the using a syringe pump (Teledyne Isco 260D, Lincoln, NE, USA). This is followed by the last (5th) zone of the extruder, and a melt pump securing constant material flow as well as a static mixer, which ensures efficient heat removal from the melt. For proper foam cell formation, a strand die with an opening of 2 mm in diameter was used. The pressure drop and the temperature on each element was continuously monitored. The main parameters for the extrusion foaming are shown in Table 2. The foamed product was uniaxially oriented for a short period of time using a precision belt puller and subsequently was left to relax and cooled in ambient conditions, reaching a final diameter of 10-12 mm and expansion ratios of 10-25. The invented technology provides the opportunity to produce anisotropic PLA foams with lens-like cells in an entirely different way from the state-of-the-art methods (e.g. biaxially stretched porous films, Fig. 1c), as the longitudinal orientation coupled with the relaxing step eventually has the opposite effect as conventional orientation methods, the cells become oriented in differing directions (i.e., perpendicular to the stretching/machine direction). A number of previous papers published in this topic discuss the reduction of Young's modulus and improvement of piezoelectric properties by extending the production process with additional steps consisting of pressure and temperature treatment accompanied by quenching in order to inflate the porous film with gas, thus increasing the thickness of the cells and the sample [56-58,69]. Using extrusion foaming followed by immediate uniaxial stretching

Table 2

Technological parameters of extrusion foaming process.

Extruder temp. zones [°C]	135-190
Screw speed [rpm]	18
Melt pump speed [rpm]	8
Melt pump temp. [°C]	130-135
Pressure before the melt pump [bar]	120-160
Temperature of static mixer [°C]	100-115
Temperature of die [°C]	95-110
Pressure at die [bar]	80-95
sc-CO ₂ injection rate [mL/min %]	2-3
sc-CO ₂ pressure [bar]	80-95
belt puller speed [m/s]	2-3

and relaxing, the aforementioned steps become redundant, as cell parameters can be optimized just by adjusting the orientation ratio.

2.2.2. Preparation of ferroelectret samples

3 mm thick circular slices were cut from the flexible strand product perpendicular to the machine direction to investigate piezoelectric properties, this way there was enough flat foam cells to be charged by the electretization treatment (poling). Prior to poling, the specimens were stored under nitrogen atmosphere in order to remove the moisture content of the foam and thereby reduce conductivity and hydrolytic degradation. Nitrogen was also found to be beneficial for the efficiency of the poling step in the literature [56–58,69]. Each specimen was then treated in a drying oven above T_g (at 75 °C) under a load of 167 g for 30 min, cooled to room temperature in 30 min, then cut in half to reach a final thickness of 500 μm . The samples were electretized using direct-current high-voltage corona charging (in a point plane arrangement: high-voltage needle electrode and earthed flat electrode without grid, point–plane distance: 5 mm, high voltage (U): 14 kV, treatment time (t): 30–60 s). Preliminary results indicated that ideal piezoelectric response can be obtained by setting these carefully optimized parameters. Furthermore, the strongest d_{33} values were obtained by placing the sample directly under the needle electrode using a separate PLA foam disk with appropriate height and diameter. The specimens were measured after electretization, and could be provided with an electrode layer on both sides (e.g. with the application of a sputter coated gold layer or a copper tape with conductive adhesive).

2.2.3. Characterization methods

SEM micrographs were obtained using a JEOL JSM-6380 LA type apparatus (JEOL Ltd., Akishima, Tokyo, Japan) at an accelerating voltage of 10 kV on specimens coated with gold in order to prevent charge build-up on the surface. The exploitation of artificial neural networks (AI) for image analysis was carried out using MaskRCNN, which was trained with the default training settings (epochs = 100, workers = 1, learning rate = 0.001). The training was performed on a high-performance PC (Nvidia RTX 3090 GPU, AMD Ryzen 5900X CPU).

Tensile and compression tests were performed on a Zwick-005 universal testing machine (Zwick GmbH & Co., KG, Ulm, Germany) equipped with a 5 kN load cell. Using the as-manufactured strand product, strain-controlled cyclic tensile test and force-controlled step cycle tests were conducted at 5 mm/s speed in both directions (grip to grip separation: $L_0 = 40$ mm). The upper limit of the controlled force was increased after every 60 cycles (i.e., 1 step) by 1 N from 3.5 N to 12.5 N, while the lower force limit remained 0.75 N throughout the entire measurement. Between each step, the specimen was allowed to recover its original shape in 60 s, hence a preloading cycle was applied at the beginning of the next measurement. Dynamic compression tests were carried out with a frequency of 0.5 Hz, an amplitude of 10 N (~100 kPa) and a duration of 300 cycles, using 4 mm high disks radially cut from the strand product. Hot pressing of 6- and 10-mm high foam specimens was carried out at 75 °C under a load of 167 g to reach a compression ratio of 33, and 60%, respectively. The hot pressed samples with a final height of 4 mm were also measured via the preceding method. The compressive moduli were calculated by the slope of the initial linear region of the stress strain curves according to ASTM D1621-16 standards. The tests were carried out at 25.0 °C and a relative humidity of 50%. For the measurement of d_{33} , copper-plated measuring electrodes were attached on either side of the stationary member (base) and movable member (crosshead) of the tensile tester, respectively. A sinusoidal load with a frequency of 1 Hz and different amplitudes (force-controlled, strain-controlled)

was applied on the electrets. The generated charge was measured using a Keithley Electrometer 6517 A (Keithley Instruments) as a function of time (i.e., the same measurement variable as of the compression test). From the force F and the charge Q accumulated on the electrodes during cyclic loading the transverse piezoelectric coefficient (i.e., sensitivity) of the sample is determined as $d_{33} = Q/F$ [68]. A Berlincourt piezometer (Piezotest PM300) was used for validation with 0.5–10 N static force (preload), and 0.25 N dynamic force at a frequency of 110 Hz.

3. Results and discussion

3.1. Morphology of the flexible PLA foam

Samples prepared by supercritical CO₂-assisted extrusion foaming were cut by a razor blade both in machine direction (longitudinal) and cross direction and the cell structure of the manufactured PLA foams were examined under scanning electron microscopy (SEM). When comparing the roughly circular (polygon) cells in the cross-section and the elongated cell shape in the longitudinal (axial) section of the product shown in Fig. 2a,b-d, respectively, a notable degree of dimensional anisotropy can be observed. There are several means to describe anisotropy ratio or aspect ratio (AR), in this study two distinct cell diameters were determined from the representative morphology analysis, with respect to the relevant (nearly axisymmetric) cell shapes. Presuming axial symmetry, two perpendicular diameters of a given cell were considered approximately equal, these are referred as radial diameter (d_r), while the third diameter measured perpendicularly to d_r is referred as axial diameter (d_a). AR is defined as the ratio between these diameters ($AR = d_a/d_r$). In this case, the spatial shape of the foam cells is similar to that of a flat disc or a lens, with ARs lower than 1. Unlike found in the scientific literature, the d_a of these lens-like cells is oriented in the machine direction. Moreover, the number of adjacent flat cells in this direction is infinite, hence the possibility of adequate tensile tests is given in the flexible direction.

A theoretical explanation for the unique morphology can be provided by taking into account the visco-elastic mechanisms during the production method. Albeit the cell nucleation and cell growth phase of the foaming process is carried out under uniaxial stress, final cell stabilization takes place a few minutes after leaving the extruder due to the good thermal insulation of the outer foam cells. During this interval, cell walls are in a hyperelastic state as the temperature at which the foaming compound exits the die ($T_f = 100$ –110 °C) is lower than the melting temperature ($T_m = 145$ –160 °C), but still above the glass transition temperature ($T_g = 55$ –65 °C) of PLA. At this stage the product was let to relax by the immediate elimination of the stretching force. As the relaxation of highly oriented PLA chains in this physical state is only hindered by the internal pressure of the gas cell, contraction of cell walls takes place in the machine direction, which effectuates the expansion of other cell walls (i.e., in the transverse direction), eventually reaching an equilibrium. A specific characteristic resulting from the aforementioned mechanism is highlighted in Fig. 2c and d, demonstrating that each cell wall is connected to one another at such an angle (Y-shaped joints) that provides macroscopic flexibility in the machine direction. Another consequence is that the proportion of axially (i.e., machine direction) oriented cell walls is negligible in the final cell structure, anticipating that the load-bearing capacity may have a flexural nature predominantly (i.e., bending of Y-shaped joints). This behavior is fundamentally different than from the irreversible compressive or tensile deformation of rigid cell walls in the conventional PLA foams. Interestingly, the working mechanism bear some resemblance to origami-

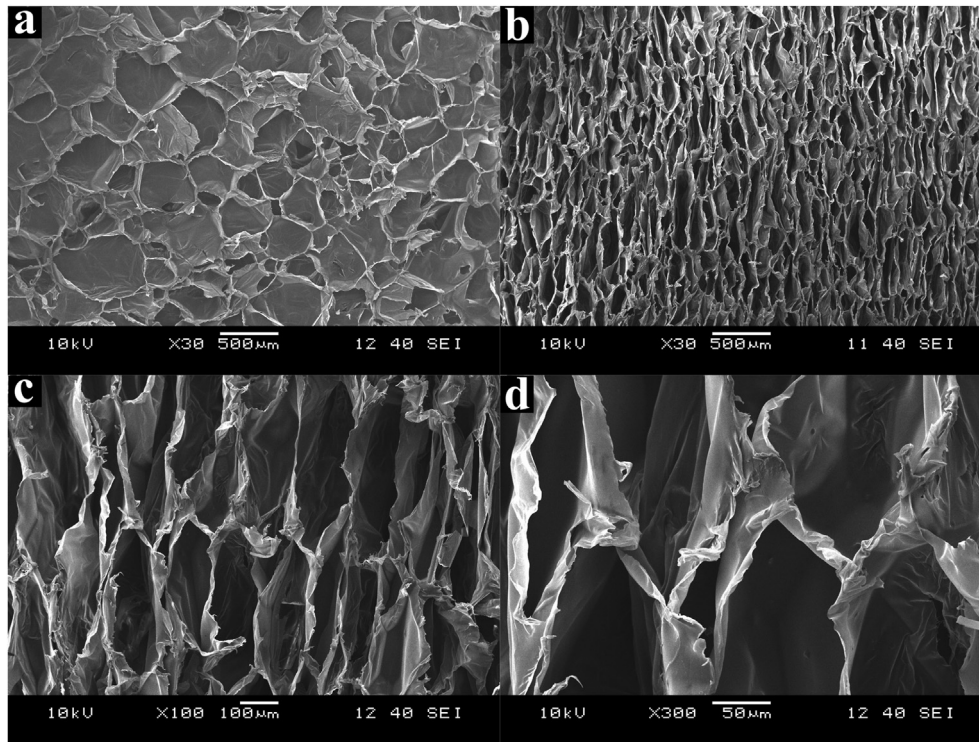


Fig. 2. SEM micrographs of the manufactured flexible PLA foam cut in the (a) cross-section (b–d) longitudinal section.

like compliant mechanisms that also enable large degrees of reversible motion of otherwise rigid materials using advanced design of flexible joints connecting rigid parts [38,65]. Further similarities can be found with structural elastic-like film (SELF) webs exhibiting an elastic-like behavior in the direction of elongation without the use of added elastic materials [66].

Besides the low aspect ratio, the relatively large width (i.e., up to 700–800 μm diameter) foam cells can also be considered advantageous in terms of flexibility, as this attribute could allow higher elongations without endangering the structural integrity of the specimen, as opposed to microcellular foams with similarly rigid cell walls.

3.2. Cyclic tensile tests

Fig. 3 shows the stress-strain curves of the dynamic tensile testing of the prepared PLA foams with a duration of 60 cycles and controlled strain between 0.2% and 10.0%. During these 60 cycles, the stress measured at 10% deformation reduced only by 17.3% (from 37.0 kPa to 30.6 kPa), an average of 0.3% in each cycle. The foam exhibited a practically linear stress-strain correlation and an unabated modulus of 352 kPa within this range.

The results of force-controlled step cycle tests are depicted in Fig. 4. Elastic strain happened to fall in the range of 10–16% in the majority of the cycles, plastic (i.e., irreversible, permanent) elongation remained under 0.06% each cycle, and an extensive range of total elongation up to 35% could be observed. The aforementioned linear stress-strain curve was typical for the 0–14% deformation range, at higher strains a steeper slope of the curve was evinced. The origin of this phenomenon can be described by structural effects. As predicted during the morphology characterization, the unique structure modifies the determinative deformation mechanism from irreversible cell damage to reversible flexural strain of bending joints. The linear elasticity and constant modulus in a relatively wide range shows the spring-like *modus operandi* of the

novel flexible foam. With regard to a rigid closed-cell foam, this finding is not expected by any means, least in the case of a cellular structure comprising of the fragile PLA polymer. The rationale behind the advanced resilience can be explained by another effect: the air cushioning phenomenon of the gas volumes entrapped in the closed-cell structure also enhances flexibility, in addition to the aforementioned structural (morphological) elasticity of thin and anisotropic cell walls. The combination of these influencing factors results in the ability of the foam to recover from extensive deformation without tensile failure exhibiting predominantly elastic strain and a minimal degree of plastic deformation. The increasing modulus at higher strain proves the recurrence of the deformation mechanism of regular closed-cell foams, as an increasing proportion of the load-bearing capacity is provided by the rigid cell walls. The flexural and tensile strength of the PLA structure was enhanced

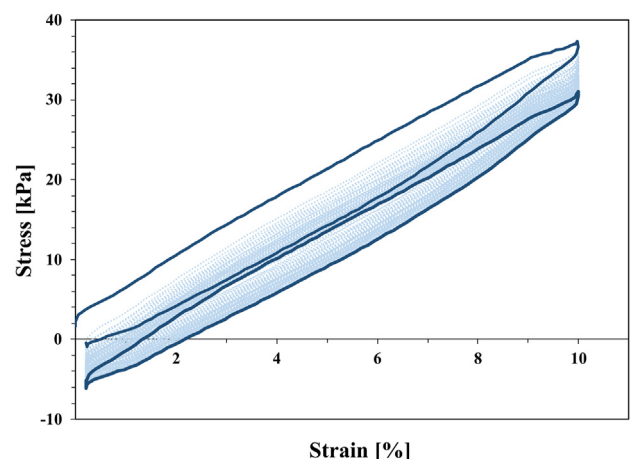


Fig. 3. Strain-controlled cyclic tensile test on flexible PLA foam (as-manufactured strand product) at 5 mm/min speed, grip to grip separation: $L_0 = 40$ mm.

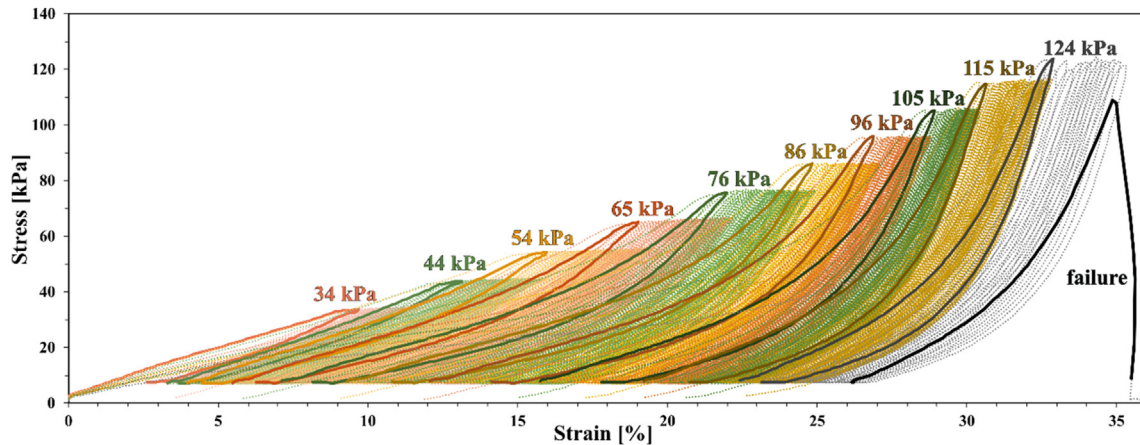


Fig. 4. Stress-controlled step cyclic tensile tests on flexible PLA foam: every 60 cycles (i.e., 1 step) the upper force limit was increased (between each step, the specimen was allowed to recover its original shape in 60 s).

by the montmorillonite (MMT) clay nanoparticles, used as nucleating agent, most certainly oriented in the plane of the cell walls [32]. The plastic deformation can be explained by gas diffusion towards the inner foam cells, as these voids encounter significantly lower pressure than the ambient atmosphere. However, when unloaded, the foam is able to partially recover this plastic elongation over time.

During cyclic loading and unloading of elastic materials, it is well known that the results deviate from Hooke's law, resulting in a non-linear correlation and different courses of loading and unloading stress-strain curves. Whenever more force (and work) is required during the loading than the unloading of the sample, the energy difference demonstrated by the area of the hysteresis loop is dissipated by physical effects and is converted into heat. Various effects can be taken into account such as friction or gas compression/decompression. Given the good thermal insulation properties of the PLA foam product, quasi-adiabatic conditions can be presumed. As a result, a larger proportion of the energy is expected to be dissipated via micromechanical friction in the cell wall joints than by means of pressure changes of the gas phase in the quasi-adiabatic system. However, compared to the moderate number of literature sources that published cyclic tensile test results, this hysteresis loop is considered to be small, a higher degree of energy

is recovered instead of being absorbed through the discussed routes.

3.3. Cyclic compression tests

Stress-strain curves of the dynamic compression tests can be inspected in Fig. 5. Under a considerable amount of compressive stress, the foam samples also exhibited highly flexible behavior, with elastic deformation around 12–14% as well as a relatively small amount of plastic deformation for each compression cycle, an average of 0.048% throughout the measurement. Given the natural effects during compression tests such as gas loss and densification of the flat foam cells, the plastic deformation was gradually decreasing from around 0.3%–0.02%.

3.4. Cyclic compression tests of hot pressed foam samples

To explore the development possibilities towards improved mechanical characteristics (resilience, energy recovery), hot pressed samples ($h = 4$ mm, compression ratios: 33% and 60%) were also measured via the preceding method, two representative stress-strain curve of which are shown in Fig. 6. On the one hand, total plastic deformation was effectively decreased by 74% and 88%

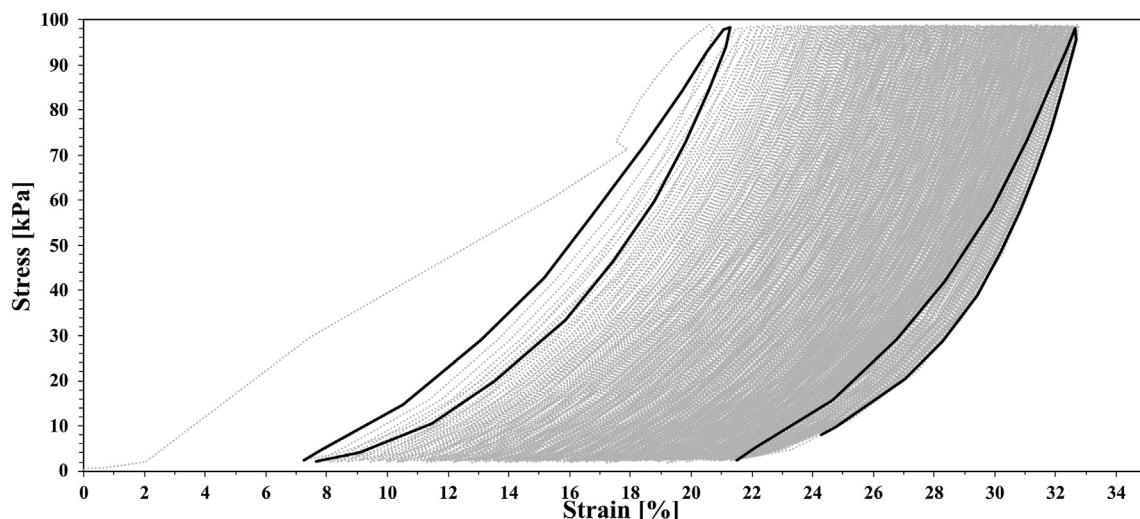


Fig. 5. Cyclic compression tests at 0.5 Hz, 10 N (~100 kPa) and 300 cycles, performed on flexible PLA foam disks radially cut from the strand product.

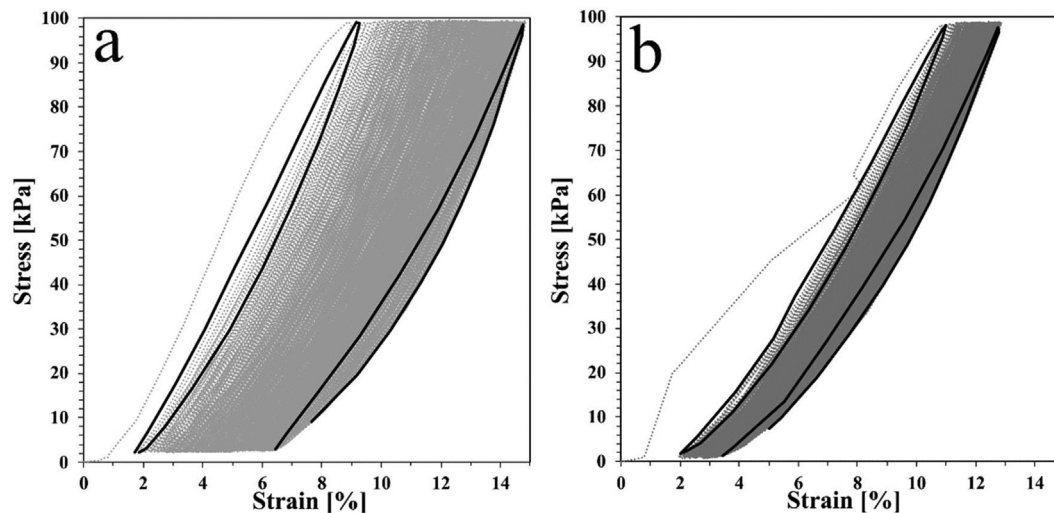


Fig. 6. Cyclic compression tests at 0.5 Hz, 10 N (~100 kPa) and 300 cycles, performed on flexible PLA foams, hot pressed at 75 °C to reach compression ratios: (a) 33% and (b) 60%.

using respective compression ratios of 33% and 60%, on the other hand, elastic strain remained around 8–9%. The compressive modulus of elasticity was found to increase from 800 kPa of the non-treated sample to 1.0–1.2 MPa due to hot pressing.

To further investigate the reasons behind this improvement, SEM images taken from the longitudinal sections of neat and

compressed foam samples are displayed in Fig. 7a–c. Depending on the compression ratio, foam cells are oriented to a different extent within the core of the sample, whilst an outer skin of incessant PLA film and randomly oriented cells can be observed on the boundary of the foam. An explanation for the skin formation could be given by considering the higher cooling rate of the PLA and limited cell

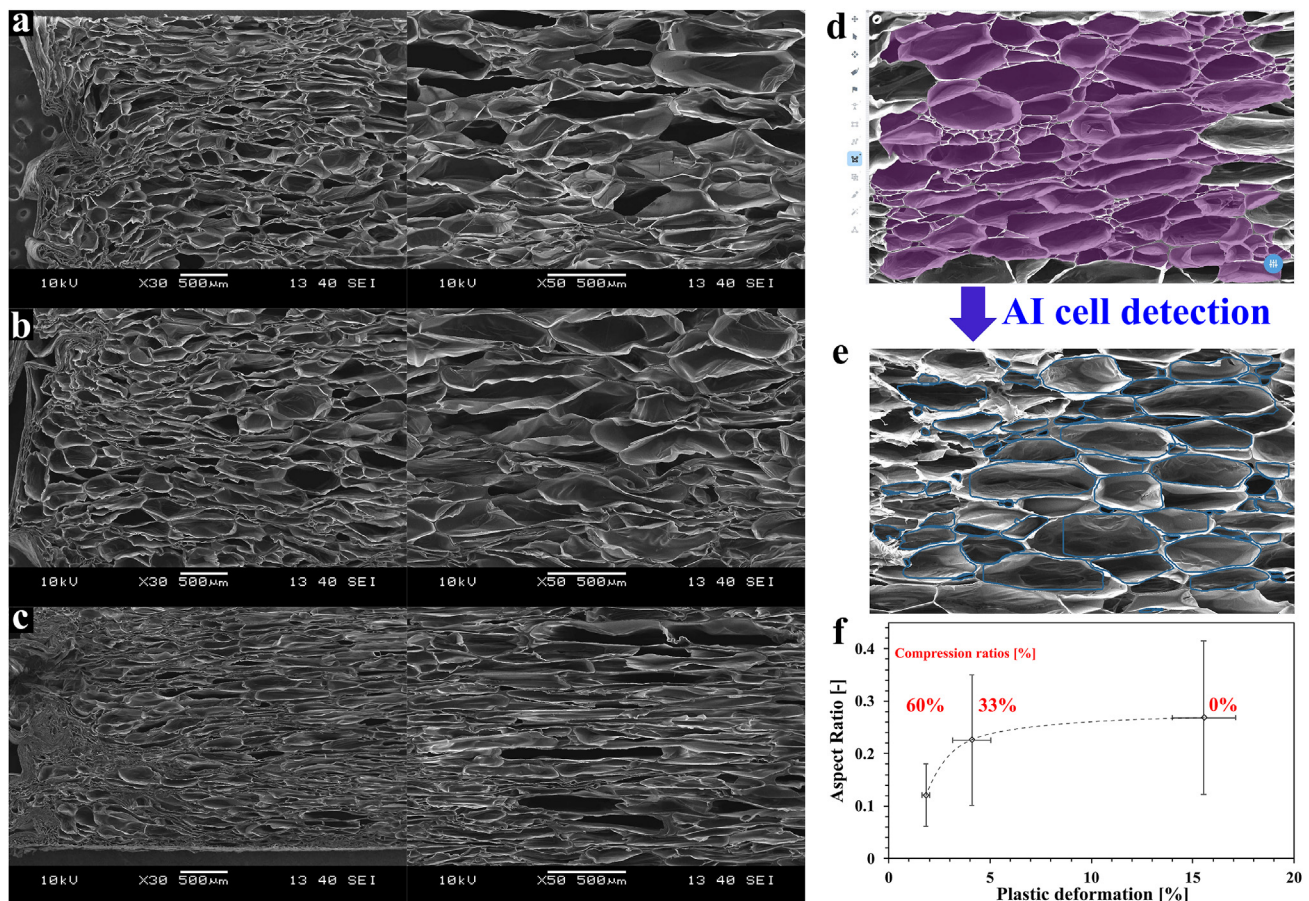


Fig. 7. SEM images of PLA foam samples with different compression ratios (a) 0% (b) 33% (c) 60% and magnifications (× 30, × 50). SEM micrographs (d) after annotation and (e) morphology analyzed by AI. (f) Correlation between plastic deformation and AR.

growth around the perimeter. During uniaxial orientation the outer skin layer stretches and solidifies, but then becomes concertinated following the immediate relaxation and axial shrinkage of the product. At the beginning of each compression test, an initial preload of 10 N was applied to eliminate the effect of this outer skin layer. The two radially cut sides of the foam disks that has been in direct contact with the hot pressing apparatus (75 °C) are more dense than the inner part of the sample, this effect can also be linked to the good thermal insulating property of the foam and the consequent temperature gradient throughout the combined compression and heat treatment. The densified layers provide an impermeable boundary similar to the skin region, thus hindering gas loss and favorably reducing permanent deformation (Fig. 6).

Cell morphology was characterized using image analysis supported by artificial neural networks (artificial intelligence, AI) on SEM images with appropriate contrast and brightness, as illustrated in Fig. 7d and e. Cells on 7 images were labelled using an on-line annotation tool [67]. The incomplete voids located on the edges of the SEM images were omitted, 1200 individual cells were labelled in total. In order to automatically multiply the training dataset, the labelled images were augmented (transformed): random rotations between 0 and 90° and random scaling between 1:1 and 1:4 were applied to the images. The cell detection was carried out using MaskRCNN, which was trained with the default training settings. The performance of the obtained model was validated by analyzing a separate set of SEM images, previously unknown to the AI. As it was shown in Fig. 7e, the system was able to differentiate between foam cells with high accuracy, although subsequent manual adjustment of the exact cell parameters was necessary. The average AR value was calculated representatively for each hot pressed sample from the d_a and d_r parameters of 260–300 cells. Correlation between resiliency (i.e., plastic deformation) and AR of the samples was evinced as depicted in Fig. 7f.

During cyclic compression tests, the samples demonstrated structural flexibility similarly to cyclic tensile tests allowing to draw

analogous conclusions: the unique microstructure modifies the deformation mechanism from cell wall collapse or concertinating towards reversible flexural strain via elastic bending of cell wall joints. In addition, mechanical properties can be further enhanced by lowering the AR via compression above T_g or by increasing the draw ratio (thus the degree of relaxation) during foam extrusion.

3.5. Electromechanical characterization

The d_{33} coefficients of electretized PLA foam samples were comprehensively studied using a Zwick-005 universal testing machine coupled with electrodes and a Keithley Electrometer 6517 A for signal detection. An example of the test results is depicted in Fig. 8. As an effect of the sinusoidal load (1 N; 1 Hz), an alternating signal can be measured in the range of –149 and –456 pC. The generated charge resembles the mechanical excitation in a sensitive manner, even smaller differences in the applied force (e.g. at 14 and 16 s) can be detected. This phenomenon points out the indirect way of calculating the d_{33} values, the larger amplitudes should be divided by their counterparts. Given that the lower measuring limit of the cyclic test is 0.1 N, the charge amplitudes are divided by force values smaller than 1 N, the resulting average d_{33} value is 320 pC/N. When compared to the mass (~9 mg) of a given ferroelectret sample, there is such an amount of charge carriers within the cellular structure, that the specimen lifts up from the bottom measuring electrode towards the upper grounded electrode. This phenomenon only happens when the sample is closer than 3–4 mm to the upper electrode, illustrating the short range of the electromechanical forces.

As evinced in the compression tests (Figs. 6 and 7) and the literature [51], the stress-strain relationship of cellular foams is not exactly linear, thus the correlation between d_{33} and load is susceptible to the microstructure. A more straightforward relationship was found between charge and strain when strain-controlled cycle measurements were conducted via increasing the deformation (i.e.,

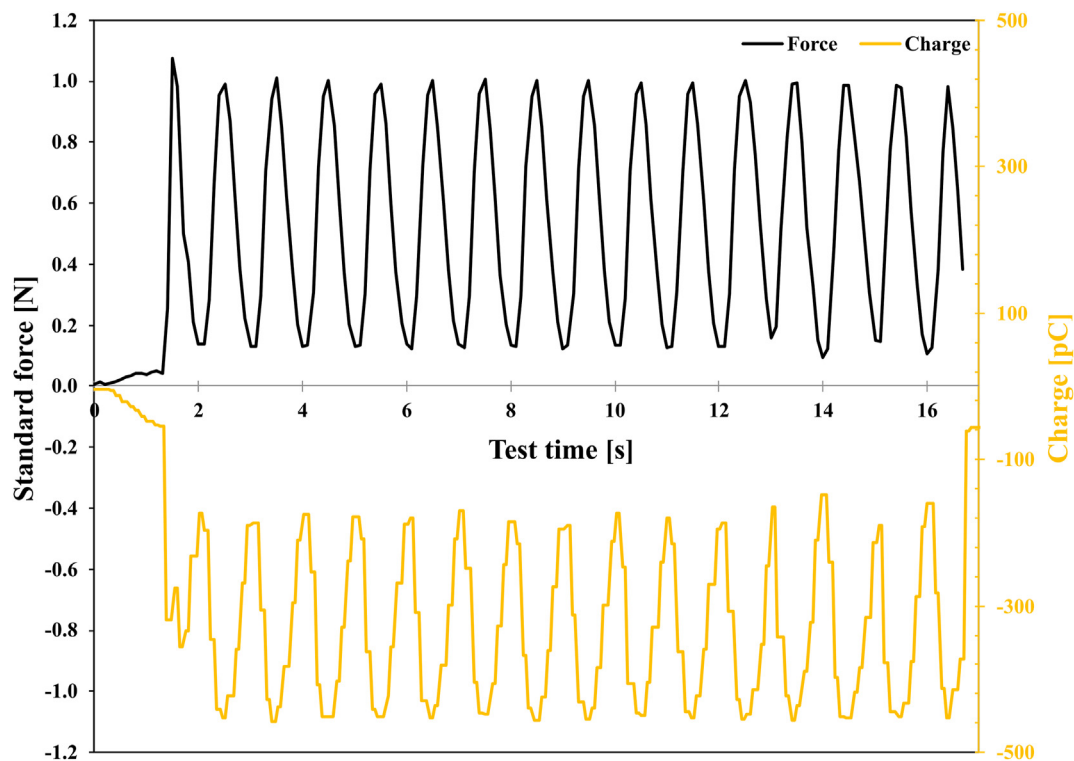


Fig. 8. Piezoelectric response (d_{33}) of the prepared PLA ferroelectret measured during force-controlled step cycle test (1 N, 1 Hz).

decreasing the gap between the electrodes) stepwise by 20 μm after every 15 cycles (Fig. 9). The results showed that the generated charge also increases stepwise, predicting a linear charge-strain relationship. The charge, d_{33} values, and standard force is depicted in Fig. 10 as functions of deformation, showing the resulting equation. The reason for this phenomenon is given in the ferroelectric mode of operation, the amount of charge induced between the opposing electrodes is directly affected by the relative distance of the charge carriers deposited on the cell walls.

For validation of the measurements, the d_{33} coefficients of the samples were also measured by Berlincourt piezometer. The best parity between d_{33} values measured by these methods were obtained at 1 N static force. The differing results at higher static forces

are not surprising, as this facile test method is optimized for solid piezoelectric materials with elastic moduli several orders of magnitude higher than the foams, and with completely different charge generating physical phenomena.

4. Conclusions

In this paper, highly flexible and piezoelectric PLA foams and their simple manufacturing methods were firstly introduced. It was shown that dimensional anisotropy offers a number of advantageous features such as structural elasticity and chargeability. The PLA foam product exhibited elastic strains ranging between 10% and 16% and a total elongation of 35% during dynamic tensile tests,

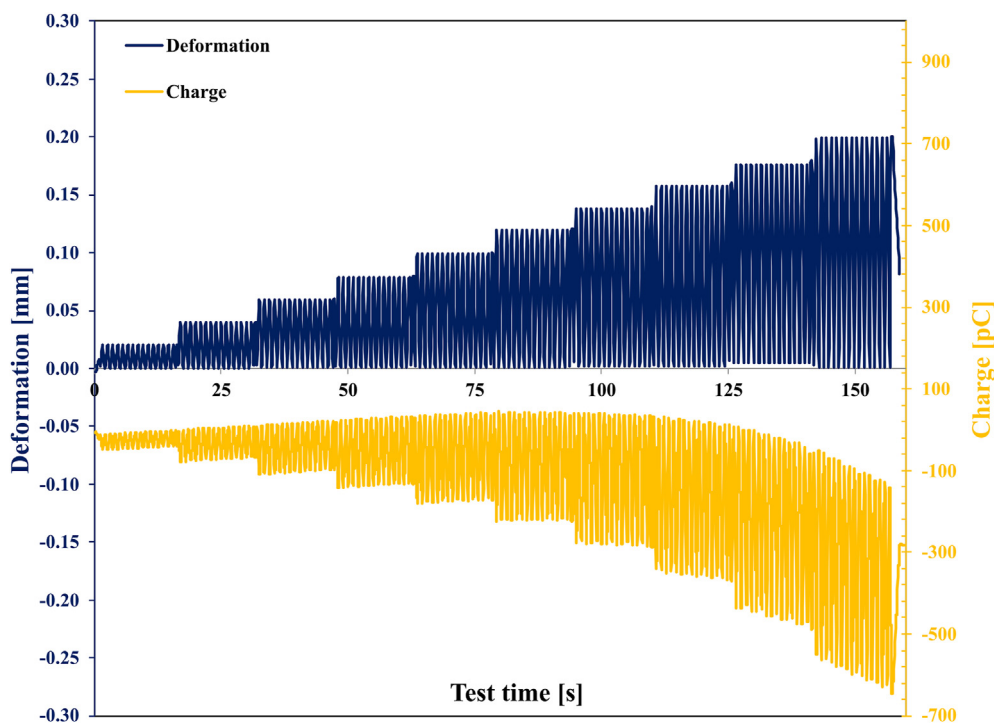


Fig. 9. Piezoelectric response (d_{33}) of the prepared PLA ferroelectric measured during strain-controlled step cycle test (0.025–0.200 mm; 1 Hz).

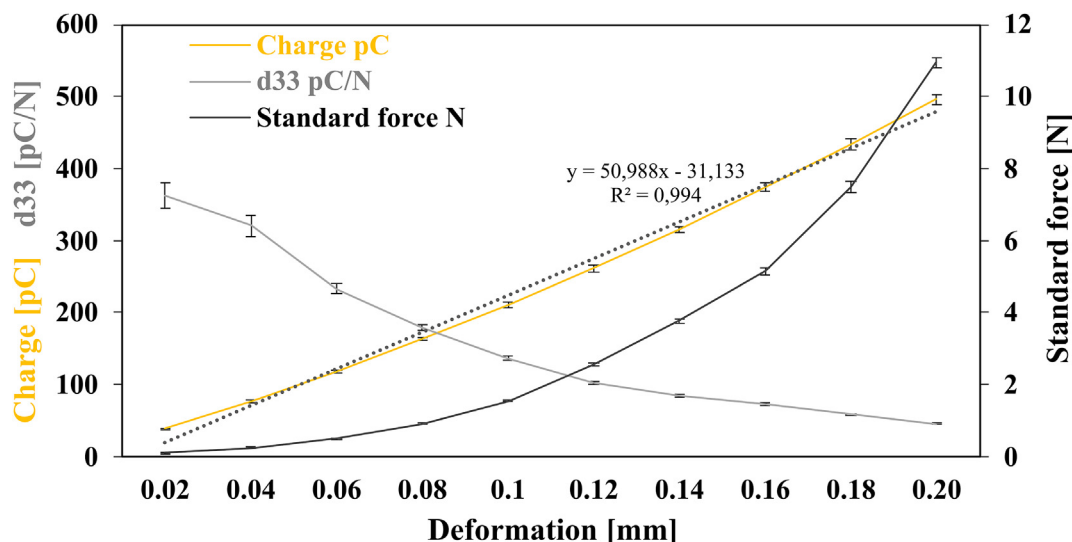


Fig. 10. Measured charge [C], standard force [N] and calculated d_{33} piezoelectric response [pC/N] of the prepared PLA ferroelectric during strain-controlled step cycle test.

revealing a performance fundamentally atypical for closed-cell foams made of rigid polymers. Electretized PLA samples comprising of the same anisotropic cellular material showed notable d_{33} values up to 320 pC/N.

The efficiency and eco-friendliness of the produced foams are crucial factors to consider for novel products to be developed utilizing their unique capabilities. The flexible and piezoelectric PLA foams presented in this study combine several advantageous properties that can make a product green. Apart from PLA's intrinsic features (renewable source, biocompatibility, trigger-biodegradability), these low-density foams use lower amounts of raw material for a given volume, consequently they demonstrate high charge/mass ratio and an unexpected degree of flexibility. Regarding the production of piezoelectret materials, a major advantage of the novel technology presented herein is that due to the simplified auxiliary equipment it requires smaller space and capital investment, and can be easily integrated in lab-scale or medium-scale manufacturing methods, as opposed to the biaxial orientation of cellular films [43]. Another feature of the new approach to extrusion foamed piezoelectrets is lower waste generation, as the samples does not need to be cut out of a biaxially oriented film, the shape and size of a given product can be defined by the foaming die design.

The newly developed highly flexible and/or piezoelectric PLA foams could be easily applicable in consumer goods requiring energy absorption or recovery, given the readily tuneable elastic modulus. When charged, the PLA foams can be used as sensors, actuators or energy harvesting generators in wireless electronic applications, within the thermal and mechanical constraints of the polymer. Furthermore, due to the biocompatibility of PLA, it is possible to develop high-tech products such as in-vivo sensors or tissue engineering scaffolds, also exploiting the electromechanical stimulation of living cells.

Declaration of competing interest

The authors declare the following financial interests/personal relationships which may be considered as potential competing interests: Gyorgy Marosi has patent #PCT/HU2021/050,065 pending to Hungarian Intellectual Property Office.

Acknowledgement

Supported by the ÚNKP-21-4 New National Excellence Program of the Ministry for Innovation and Technology from the source of the National Research, Development and Innovation Fund. Financed from the NRDI fund in the frame of 2019–1.3.1- KK-2019–0 0 0 04 project. The research was funded by the Hungarian Scientific Research Fund, grant number FK128352. The work was partly supported by the National Research, Development and Innovation Fund of the Hungarian Government in the framework of KoFAH, NVKP_16-1-2016-0018 project.

References

- [1] R. Mi, T. Li, D. Dalgo, C. Chen, Y. Kuang, S. He, X. Zhao, W. Xie, W. Gan, J. Zhu, J. Srebric, R. Yang, L. Hu, A clear, strong, and thermally insulated transparent wood for energy efficient windows, *Adv. Funct. Mater.* 30 (1) (2020).
- [2] David Feber, Stefan Helmcke, Thomas Hundertmark, Chris Musso, Wen Jie Ong, Osgaard Jonas, Jeremy Wallach, Climate Impact of Plastics, McKinsey & Co, 2022.
- [3] E.T.H. Vink, S. Davies, Life cycle inventory and impact assessment data for 2014 Ingeo® polylactide production, *Ind. Biotechnol.* 11 (3) (2015) 167–180.
- [4] M.F. Cosate de Andrade, P.M.S. Souza, O. Cavalett, A.R. Morales, Life cycle assessment of poly(lactic acid) (PLA): comparison between chemical recycling, mechanical recycling and composting, *J. Polym. Environ.* 24 (4) (2016) 372–384.
- [5] E. Castro-Aguirre, F. Iniguez-Franco, H. Samsudin, X. Fang, R. Auras, Poly(lactic acid)—mass production, processing, industrial applications, and end of life, *Adv. Drug Deliv. Rev.* 107 (2016) 333–366.
- [6] S. Walker, R. Rothman, Life cycle assessment of bio-based and fossil-based plastic: A review, *J. Clean Prod.* 261 (2020).
- [7] C. Ingrao, C. Tricase, A. Cholewa-Wójcik, A. Kawecka, R. Rana, V. Siracusa, Poly(lactic acid) trays for fresh-food packaging: a Carbon Footprint assessment, *Sci. Total Environ.* 537 (2015) 385–398.
- [8] D. Maga, M. Hiebel, N. Thonemann, Life cycle assessment of recycling options for polylactic acid, *Resour. Conserv. Recycl.* 149 (2019) 86–96.
- [9] S. Spierling, V. Venkatachalam, M. Madersbach, N. Becker, C. Herrmann, H.J. Endres, End-of-life options for bio-based plastics in a circular economy—status quo and potential from a life cycle assessment perspective, *Resources* 9 (7) (2020).
- [10] M.P. Desole, C. Aversa, M. Barletta, A. Gisario, A. Vosooghnia, Life cycle assessment (LCA) of PET and PLA bottles for the packaging of fresh pasteurised milk: the role of the manufacturing process and the disposal scenario, *Packag. Technol. Sci.* 35 (2) (2022) 135–152.
- [11] S. Farah, D.G. Anderson, R. Langer, Physical and mechanical properties of PLA, and their functions in widespread applications — a comprehensive review, *Adv. Drug Deliv. Rev.* 107 (2016) 367–392.
- [12] X. Qi, Y. Ren, X. Wang, New advances in the biodegradation of Poly(lactic acid), *Int. Biodeterior. Biodegrad.* 117 (2017) 215–223.
- [13] M.A. Schuetz, L.R. Glicksman, A Basic Study of Heat Transfer Through Foam Insulation 20 (2) (1984) 114–121, <https://doi.org/10.1177/0021955X8402000203>.
- [14] V. Bernardo, E. Laguna-Gutierrez, A. Lopez-Gil, M.A. Rodriguez-Perez, Highly anisotropic crosslinked HDPE foams with a controlled anisotropy ratio: production and characterization of the cellular structure and mechanical properties, *Mater. Des.* 114 (2017) 83–91.
- [15] M. Antunes, V. Realinho, J.L. Velasco, E. Solórzano, M.A. Rodríguez-Pérez, J.A. de Saja, Thermal conductivity anisotropy in polypropylene foams prepared by supercritical CO₂ dissolution, *Mater. Chem. Phys.* 136 (1) (2012) 268–276.
- [16] L.J. Gibson, M.F. Ashby, *Cellular Solids: Structure and Properties*, Cambridge University Press, 1997.
- [17] K. Larsen, Recycling wind turbine blades, *Renewable Energy Focus* 9 (7) (2009) 70–73.
- [18] C. Kaboglu, S. Pimenta, A. Morris, J.P. Dear, The effect of different types of core material on the flexural behavior of sandwich composites for wind turbine blades, *J. Therm. Eng.* 3 (2) (2017) 1102–1109.
- [19] A. Al-Hamdan, M. Al-Ajlani, M. Alhusein, C.D. Rudd, A.C. Long, Behaviour of core materials during resin transfer moulding of sandwich structures, *Mater. Sci. Technol.* 16 (7–8) (2000) 929–934.
- [20] M. Tomin, Á. Kmetty, Polymer foams as advanced energy absorbing materials for sports applications—a review, *J. Appl. Polym. Sci.* 139 (9) (2022).
- [21] P. Yongyan, Z. Wenge, W. Minghui, C. Yiyu, W. Fei, CN11621054A Micro-cellular Foam Material and Preparation Method Thereof, 2020 issued 2020.
- [22] D. Eaves, *Handbook of Polymer Foams*, Smithers Rapra Technology, 2004.
- [23] Y. Di, S. Iannace, E. di Maio, L. Nicolais, Reactively modified poly (lactic acid): properties and foam processing, *Macromol. Mater. Eng.* 290 (11) (2005) 1083–1090.
- [24] M. Nofar, C.B. Park, Poly (lactic acid) foaming, *Prog. Polym. Sci.* 39 (10) (2014) 1721–1741.
- [25] S.T. Lee, L. Kareko, J. Jun, Study of thermoplastic PLA foam extrusion, *J. Cell. Plast.* 44 (4) (2008) 293–305.
- [26] R. Auras, L. Lim, S. Selke, H. Tsuji, *Poly (Lactic Acid): Synthesis, Structures, Properties, Processing, and Applications* (Wiley Series on Polymer Engineering and Technology Book 6), Wiley, 2011.
- [27] Q. Yaxin, L. Qiaolian, W. Defeng, X. Wenyuan, P. Sheng, L. Ruyue, X. Hui, Cyclic tensile properties of the polylactide nanocomposite foams containing cellulose nanocrystals, *Cellulose* 25 (2018) 1795–1807.
- [28] M. Meller, J. Li, J. Dolega, ES2610928T3 - Foam Material with Very Low Thermal Conductivity and Process for its Production, 2017 issued 2017.
- [29] S. Nagata, K. Koyama, New method for estimating the cellular structure of plastic foams based on dielectric anisotropy, *Polym. Eng. Sci.* 39 (5) (1999) 896–903.
- [30] A.T. Huber, L.J. Gibson, Anisotropy of foams, *J. Mater. Sci.* 23 (8) (1988) 3031–3040.
- [31] M. Floren, S. Spilimbergo, A. Motta, C. Migliarese, Porous poly(D, L-lactic acid) foams with tunable structure and mechanical anisotropy prepared by supercritical carbon dioxide, *J. Biomed. Mater. Res. B Appl. Biomater.* 99 B (2) (2011) 338–349.
- [32] M. Antunes, J.L. Velasco, V. Realinho, E. Solórzano, Study of the cellular structure heterogeneity and anisotropy of polypropylene and polypropylene nanocomposite foams, *Polym. Eng. Sci.* 49 (12) (2009) 2400–2413.
- [33] J. Chen, L. Yang, D. Chen, Q. Mai, M. Wang, L. Wu, P. Kong, Cell structure and mechanical properties of microcellular PLA foams prepared via autoclave constrained foaming, *Cell. Polym.* 40 (3) (2020) 101–118.
- [34] R.E. Lee, Y. Guo, H. Tamber, M. Planeta, S. Ning, S. Leung, Thermoforming of Poly(lactic Acid) Foam Sheets: Crystallization Behaviors and Thermal Stability, 2016.
- [35] A. Rizvi, R.K.M. Chu, C.B. Park, Scalable fabrication of thermally insulating mechanically resilient hierarchically porous polymer foams, *ACS Appl. Mater. Interfaces* 10 (44) (2018) 38410–38417.

- [36] T.R. Kuang, H.Y. Mi, D.J. Fu, X. Jing, B.Y. Chen, W.J. Mou, X.F. Peng, Fabrication of poly(lactic acid)/graphene oxide foams with highly oriented and elongated cell structure via unidirectional foaming using supercritical carbon dioxide, *Ind. Eng. Chem. Res.* 54 (2) (2015) 758–768.
- [37] N.J. Mills, H.X. Zhu, The high strain compression of closed-cell polymer foams, *J. Mech. Phys. Solid.* 47 (3) (1999) 669–695.
- [38] L.L. Howell, *Compliant Mechanisms*, 21st Century Kinematics, 2013, pp. 189–216.
- [39] R.E. Lee, Y. Guo, H. Tamber, M. Planeta, N.S.S. Leung, Thermoforming of polylactic acid foam sheets: crystallization behaviors and thermal stability, *Ind. Eng. Chem. Res.* 55 (3) (2016) 560–567.
- [40] Dániel Vadas, Igricz Tamás, Katalin Bordácsné Bocz, and Marosi György (2022) WO2022118053A1. issued 2022.
- [41] H. Abbasi, M. Antunes, J.I. Velasco, Recent advances in carbon-based polymer nanocomposites for electromagnetic interference shielding, *Prog. Mater. Sci.* 103 (2019) 319–373.
- [42] X. Zhang, Z. Li, K. Liu, L. Jiang, Bioinspired multifunctional foam with self-cleaning and oil/water separation, *Adv. Funct. Mater.* 23 (22) (2013) 2881–2886.
- [43] Kari Kirjavainen (1987) US4654546. issued 1987.
- [44] M. Paajanen, J. Lekkala, K. Kirjavainen, ElectroMechanical Film (EMFi) – a new multipurpose electret material, *Sensor. Actuator.* 84 (2000) 95–102.
- [45] G.S. Neugschwandtner, R. Schwödauier, M. Vieytes, S. Bauer-Gogonea, S. Bauer, J. Hillenbrand, R. Kressmann, G.M. Sessler, M. Paajanen, J. Lekkala, Large and broadband piezoelectricity in smart polymer-foam space-charge electrets, *Appl. Phys. Lett.* 77 (23) (2000) 3827–3829.
- [46] K. Kapat, Q.T.H. Shubhra, M. Zhou, S. Leeuwenburgh, Piezoelectric nanobiomaterials for biomedicine and tissue regeneration, *Adv. Funct. Mater.* 30 (44) (2020).
- [47] M.T. Chorsi, E.J. Curry, H.T. Chorsi, R. Das, J. Baroody, P.K. Purohit, H. Ilies, T.D. Nguyen, Piezoelectric biomaterials for sensors and actuators, *Adv. Mater.* 31 (1) (2019), 1802084.
- [48] G.M. Sessler, *Electrets*, Springer Berlin Heidelberg, 1987.
- [49] A. Savolainen, K. Kirjavainen, Electrothermomechanical film.: Part I. Design and characteristics, *J. Macromol. Sci. Part A - Chemistry* 26 (2–3) (1989) 583–591.
- [50] P. Zhang, Z. Xia, X. Qiu, F. Wang, X. Wu, Influence of charging parameters on piezoelectricity for cellular polypropylene film electrets, 12th International Symposium on Electrets 2 (1) (2005) 39–42.
- [51] J. Hillenbrand, G.M. Sessler, High-sensitivity piezoelectric microphones based on stacked cellular polymer films (L), *J. Acoust. Soc. Am.* 116 (6) (2004) 3267–3270.
- [52] H. Ohigashi, Electromechanical properties of polarized polyvinylidene fluoride films as studied by the piezoelectric resonance method, *J. Appl. Phys.* 47 (3) (1976) 949–955.
- [53] W. Künstler, Z. Xia, T. Weinhold, A. Pucher, R. Gerhard-Mulhaupt, Rapid communication Piezoelectricity of porous polytetrafluoroethylene single- and multiple-film electrets containing high charge densities of both polarities, *Appl. Phys.* 70 (2000) 5–8.
- [54] M. Paajanen, J. Lekkala, H. Valimäki, Electromechanical modeling and properties of the electret film EMF1, *IEEE Trans. Dielectr. Electr. Insul.* 8 (4) (2001).
- [55] G.S. Neugschwandtner, R. Schwödauier, S. Bauer-Gogonea, S. Bauer, M. Paajanen, J. Lekkala, Piezo- and pyroelectricity of a polymer-foam space-charge electret, *J. Appl. Phys.* 89 (8) (2001) 4503–4511.
- [56] X. Zhang, J. Hillenbrand, G.M. Sessler, Piezoelectric d33 coefficient of cellular polypropylene subjected to expansion by pressure treatment, *Appl. Phys. Lett.* 85 (7) (2004) 1226–1228.
- [57] M. Wegener, W. Wirges, J. Fohlmeister, B. Tiersch, R. Gerhard-Mulhaupt, Two-step inflation of cellular polypropylene films: void-thickness increase and enhanced electromechanical properties, *J. Phys. D Appl. Phys.* 37 (4) (2004) 623–627.
- [58] M. Wegener, W. Wirges, R. Gerhard-Mulhaupt, M. Dansachmüller, R. Schwödauier, S. Bauer-Gogonea, S. Bauer, M. Paajanen, H. Minkinen, J. Raukola, Controlled inflation of voids in cellular polymer ferroelectrets: optimizing electromechanical transducer properties, *Appl. Phys. Lett.* 84 (3) (2004) 392–394.
- [59] X. Qiu, M. Wegener, W. Wirges, X. Zhang, J. Hillenbrand, Z. Xia, R. Gerhard-Mulhaupt, G.M. Sessler, Penetration of sulfur hexafluoride into cellular polypropylene films and its effect on the electric charging and electromechanical response of ferroelectrets, *J. Phys. D Appl. Phys.* 38 (4) (2005) 649–654.
- [60] Masamichi Ando, and Takafumi Inoue (2014) EP2899615A1. issued 2014.
- [61] Hiroshi Koike, Seiichiro Iida, Hidekazu Kodama, Yoshinobu Yasuno, and Eiichi Fukada (2016) US9381724B2. issued 2016.
- [62] S. Zhukov, X. Ma, H.von Seggern, G.M. Sessler, O. ben Dali, M. Kupnik, X. Zhang, Biodegradable cellular polylactic acid ferroelectrets with strong longitudinal and transverse piezoelectricity, *Appl. Phys. Lett.* 117 (11) (2020).
- [63] O.B. Dali, S. Zhukov, M. Rutsch, C. Hartmann, H. von Seggern, G.M. Sessler, M. Kupnik, Biodegradable 3D-printed ferroelectret ultrasonic transducer with large output pressure, *IEEE International Ultrasonics Symposium, IUS (2021) 1–4*, in: <https://ieeexplore.ieee.org/xpl/conhome/9593294/proceeding?isnumber=9593298&sortType=vol-only-seq&refinementName=Author&refinements=Author:Omar%20Ben%20Dali>.
- [64] S. Gong, B. Zhang, J. Zhang, Z.L. Wang, K. Ren, Biocompatible poly(lactic acid)-based hybrid piezoelectric and electret nanogenerator for electronic skin applications, *Adv. Funct. Mater.* 30 (14) (2020).
- [65] B. Sargent, J. Butler, K. Seymour, D. Bailey, B. Jensen, S. Magleby, L. Howell, An origami-based medical support system to mitigate flexible shaft buckling, *J. Mech. Robot.* 12 (4) (2020), 041005.
- [66] Roe, D.C., Goulait, D.J.K., Rodriguez, S.S., and Cabell, D.W. (1999) US5876391A. issued 1999.
- [67] www.supervise.ly.
- [68] R. Schwödauier, G.S. Neugschwandtner, K. Schratlbauer, M. Lindner, M. Vieytes, S. Bauer-Gogonea, S. Bauer, Preparation and characterization of novel piezoelectric and pyroelectric polymer electrets, *IEEE Transactions on Dielectrics and Electrical Insulation* 7 (4) (2000).
- [69] X. Zhang, J. Hillenbrand, G.M. Sessler, Improvement of piezoelectric activity of cellular polymers using a double-expansion process, *J. Phys. D Appl. Phys.* 37 (15) (2004) 2146–2150.